Characterization of polymer microstructures for in vitro and in vivo applications

Szabó Ágnes

Theses of the Ph.D. Dissertation

Supervisor: Dr. Fekete Zoltán

Pázmány Péter Catholic University
Faculty of Information Technology and Bionics
Roska Tamás Doctoral School of Sciences and Technology

Budapest, 2022

1 Introduction

Neural interfaces are used in fundamental research and clinical practice helping to understand brain mechanisms and to identify pathological changes that can imply clinical diagnosis. These interfaces can be either sensors, like electrophysiological recorders, or actuators like the clinically used brain pacemaker. In both cases one of the key issues is how we can mitigate the inflammatory response of the surrounding tissue, which deteriorates the long-term functionality of implants. During the development of neural implants, minimal invasiveness is an increasingly important aspect. New devices are proposed from a versatile, soft, flexible material that not only reduces the immune response of the brain tissue but also allows the combination of multiple imaging techniques. These new devices are mostly manufactured from different types of polymers. Using polymer devices fabricated with MEMS technologies is popular due to their biocompatibility, easy fabrication with soft lithography, the low cost and rapid prototyping methods available in plastic material [1].

A foreign body interaction, such as electrode insertion, provokes a complex response called reactive gliosis. The complex process involving cell division and cell migration causes the formation of a glial scar that separates the damaged tissue from the intact. Astrocytes play an important role in the evolution of the glial scar [2]. One effective method to moderate the inflammatory tissue response, based on his-

tological studies, is to reduce the mechanical mismatch between the interface materials and tissue properties [3]. Many different material combinations were published and also reviewed the most commonly used polymers for implantables [4, 5, 6]. From the most popular materials this thesis introduce application of SU-8 [7] and Parylene HT [8].

Engineering the substrate topography can improve cell-surface interaction and helps to control cell function [9, 10]. This topographical modification of the substrate is based on the crucial role of the microenvironment in cell adhesion, guidance and scaffolding [11]. Based on these phenomenons, the first thesis group examines the interaction between astrocytes and topographically structured SU-8 based surfaces. This work is fundamental research in developing neural interfaces, like electrophysiological recorders.

Several neuroimaging techniques are used to record neural activity and to map brain connectivity [12]. Electrocorticogram (ECoG) is an electrophysiological recording type, where the electrodes are placed on top of the cortex, under the skull [13]. Although ECoG needs surgical implantation, the parameters of signal quality, longevity, and reliability are advantageous compared to the most commonly used electroencephalography (EEG). Another neuroimaging technique is fluorescence microscopy which allows the examination of intact brain tissue [14]. Before the examination, fluorescent dyes are used to label the cells so the cells can be visualized. One of these fluores-

cent microscope methods is two-photon microscopy. This method is a laser-scanning technique, where near-infrared light excites the fluorescent labels using two photons, so lower energy and smaller volume are required compared to other fluorescent microscope techniques [15]. Two-photon microscopy indirectly detects the cellular changes, so combining it with electrophysiology allows connecting these changes with physiological measures. During the design of such a multimodal experiment, it is important to consider the parameters of the imaging technique that may have an effect on the other modality. The two main requirements from the ECoG device are (1) to be transparent to provide an optical window for the imaging, and (2) to hold conductive layers that help to minimize photoartefacts upon laser exposure if located in the field of view. These requirements are studied in the second thesis group in the case of a Parylene HT/ITO/Parylene HT based microECoG array with two-photon Ca2+ imaging.

2 New Scientific Results

First thesis group

I investigated the interaction of micropatterned SU-8 surface - 2 or 5 μm in diameter micropillars with an inter-pillar distance of 3/5/10 μm, 2 or 5 μm wide microsrtipes, spaced 3/5/10 μm and micromeander with the width of 2 or 5 μm and 5 μm spacing - and primer mice astrocytes with a custom-made automatic detection program on fluorescent microscope images after 24 and 48 hours of the seeding.
Corresponding publications: [J1], [C1]

Thesis 1.1. *I counted the cell numbers and the area of the nuclei on different patterns with different fixation times. I showed based on the cell numbers compared to the control that after 48 hours more cells are detected over any patterned SU-8 surface than over the flat* SiO_2 *surface. The average nucleus area in the presence of microstripes and micropillars is smaller than on a smooth* SiO_2 *surface. I examined the cell numbers together with the average nucleus size and I found that the cells adhered to the patterned surface to a greater extent than to the flat control surface, but the patterns caused a smaller nucleus size.*

SU-8, a biocompatible epoxy-based negative photoresist has been formed on a silicon surface. The different microstructures were pat-

terned by standard photolithography. The created patterns are 5.7 μm high. Micropillars are columnar structures 2 or 5 μm in diameter with an inter-pillar distance of 3/5/10 μm. Microstripes are stripes 2 or 5 μm wide, spaced at 3/5/10 μm. Micromeander consists of parallel curved stripes where the width is 2 or 5 μm and the spacing of trench is 5 μm. These three types of pattern are organized on chips of 7.1 by 7.1 mm, which also contain smooth, unpatterned areas of SiO_2 as control surfaces. Primer mouse astrocytes were seeded to the patterned chip at the Department of Physiology and Neurobiology, Faculty of Science, Eötvös Lóránd University (ELTE TTK) by Hanna Liliom and Katalin Schlett. After the fixation by 24 and 48 hours, the nuclei were stained. The DNA bonded DAPI, fluorescence stain was used. For statistical data collection, I developed a Matlab based program.

To investigate how astrocytes can attach to the surface, the cell number was counted and normalized to the smooth SiO_2 control surface belonging to the specific parameter size pattern. The bars on Figure1(1) represent the cell number rate between the control (SiO_2) surface and the patterned surface (SU-8). With this method, I compensated the different cell densities between samples. Since the area of the nuclei reflects the spreading of cells on a given surface and nucleus detection is more precise and can be easily automated, the average nucleus area was measured and normalized to the control surface. The results are shown in Figure1(2). The comparison of the cell nuclei on micromeander and on the microstripes showed no differ-

ence in the trends.

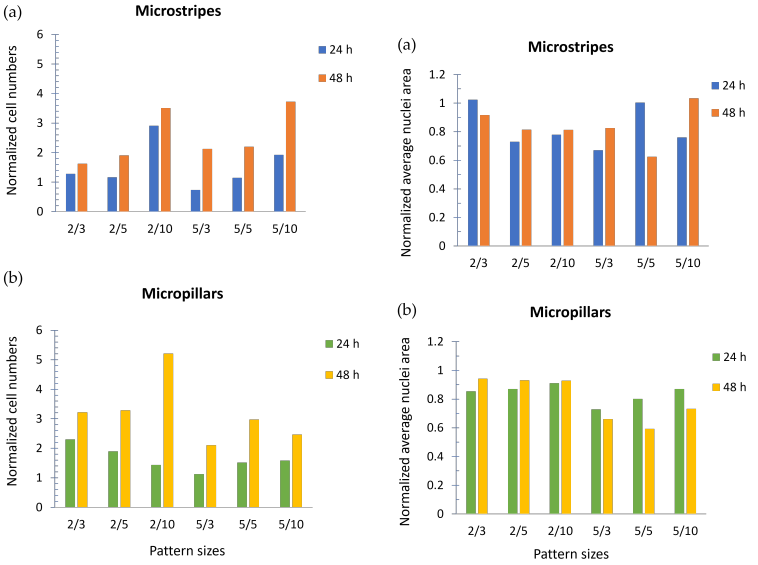

(1) Cell numbers (2) Nuclei area

Figure 1: Cell numbers (1) and average nuclei area (2) normalized to the control surface. Along the x-axis, columns are labeled in the following way: the first number indicates microstripes or micropillars width while spacing is represented by the second number (all in µm).

Thesis 1.2. *I studied the orientation of the cell nuclei and I found that microstripes force more than 50% of the cells to accommodate the pattern at an angle less than 15° with respect to pattern direction in case of all used spacing size with 2 µm wide microstripes both after 24 and 48 hours. In the case of the 5 µm wide microstripes, the 5 and 10 µm*

spacing align the cell nucleus after 24 hours, and this alignment happens for all three examined spacing after 48 hours. The 2 µm wide microstripes with 10 µm spacing have the greatest effect on orientation after the cell adhesion. Patterns with micropillars have no major effect on astrocyte nuclei compared to a smooth control surface.

The orientation of the cells is one of the most important parameters in the case of the research of engineered culturing surfaces. There are a number of studies on the cytoskeleton alignment [16, 17, 18], but the alignment of the cell nucleus is a rarely addressed question. Although it gives less information about the cell, the automation of nuclei detection is an easier task than automating the detection of the cytoskeleton, because of their more uniform shape.

The orientation is the angle between the nucleus main axis and the pattern direction, as it is used in a previous study [19]. The lines of the microstripes unambiguously define the direction, the x-axis. In the case of micropillars, the horizontal line (x-axis) was defined as the reference line of the orientation. Based on a previous study [20], we considered these cells with less than 15° orientation angle as aligned cells. Figure 2(1)-(2) show the cumulative rate of orientation in case of microstripes. It is visible that more than 50% of the cells aligned to the pattern in less than 15° angle. In the presence of micropillars 2(3)-(4), the angle distribution is even, so there is no favored topography that would alter the direction of the nuclei growth.

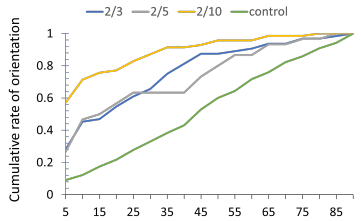

(1) 2 µm wide microstripes

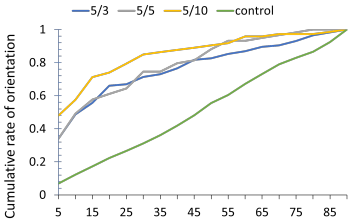

(2) 5 µm wide microstripes

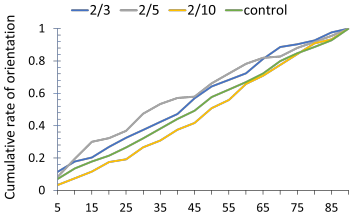

(3) 2 µm in diameter micropillars

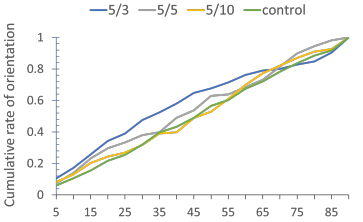

(4) 5 µm in diameter micropillars

Figure 2: Cumulative rate of orientation after 24 hours. Microstripes (1)-(2) force more than 50% of the cells to accommodate the pattern at an angle less than 15°, while in the presence of micropillars (3)-(4), the angle distribution is even, so there is no favored topography that would alter the direction of the nuclei growth.

Thesis 1.3. *The elongation rate was examined with grooves, pillars, and meander pattern and I found that the surfaces with linear elements as the microstripes, and micromeander elongate astrocyte nuclei by both 2 and 5 µm pattern width and 5 µm spacing. The results con-*

firmed that the morphology of the nucleus is an appropriate indicator to examine the effect of micropattern surfaces on cell culture evolution.

The cell nucleus is especially sensitive to changes in its microenvironment. Table 1. shows the nuclei elongation rate after 2 days. I defined the elongated elements as the nuclei that have at least 0.5 eccentricity value. The eccentricity is derived from the major axis length (Major AL) and minor axis length (Minor AL) of the ellipse that has the same normalized second central moments as the nucleus (delimiting ellipse), as in [21]. The represented rate originates from the cumulative density of the eccentricity values of the nuclei. The numbers on Table 1 show the rate of the nuclei that have greater than 0.5 eccentricity values. I compared the elongation rate between the 2 µm wide microstripes, 2 µm diameter micropillars and 2 µm wide micromeander data with 5 µm spacing (2/5) and also the different pattern types with 5 µm pattern width (and diameter in case of micropillars) and 5 µm spacing (5/5). These two parameter combinations were created with all three pattern types.

	Microstructures						
Pattern size/ spacing		Microstripes		Micropillars		Micromeander	
		pattern	*control*	*pattern*	*control*	*pattern*	*control*
	2/5	0.94	0.80	0.86	0.82	0.92	0.84
	5/5	0.93	0.87	0.88	0.72	0.94	

Table 1: Ratio of elongated nuclei in the presence of different microstructures. We defined elongated nuclei as the nuclei that have greater that 0.5 eccentricity value.

Second thesis group

A transparent microECoG device with Parylene HT as a biocompatible polymer substrate and encapsulation material with indium-tin-oxide (ITO) as a conductive layer was presented. I investigated the optical properties and photoelectric artefacts with concurrent two-photon microscope imaging.
Corresponding publication: [J2]

Thesis 2.1. *I measured the optical distortion of the device that appeared on the microscope images. The measured fluorescent microbeads with a 6 µm nominal size were not distorted in the presence of the device (control: 6.11 µm (SD=0.18 µm), covered: 6.06 µm (SD=0.16 µm), p>0.05, n=10). The quality of two-photon imaging of* Ca^{2+} *signals in hippocampal slices was performed. Cells in the CA1 subregion were*

clearly visible together with fine dendritic structures in the stratum radiatum when slices were covered with the ECoG array. The mean size of the neurites under the array was 2.17 µm (SD=0.89 µm) (n=26), while without the array, the mean size of the neurites was 1.73 µm (SD=0.61 µm) (n=29).

In order to define the optical distortion of the polymer substrate and indium-tin-oxide, two-photon images were recorded with and without fully fabricated but nonfunctional microelectrode arrays placed on fluorescent microbeads. 6 µm beads (P7220, ThermoFisher) were sealed between two glass coverslips and used for comparison of spatial resolution. Point Spread Function (PSF) was calculated as the FWHM of the gaussian fit of the microbead profile and corrected for the microbead size, and normalized to the average PSF size of control beads (Figure 3 a). Analysis of images was performed with the Matlab-based MES program (Femtonics Ltd.). Mann-Whitney U-test was used to compare apparent bead size between groups of fluorescent microbeads (n=10) with or without the presence of Parylene HT/ITO structure.

A similar test was performed ex vivo, on hippocampal slices. Two-photon images of the CA1 region of the hippocampus were recorded with and without microelectrode arrays. The diameter of all neurites in the field of view were measured and analysed (Figure 3 b). The fluorescence images were analyzed with a custom-made Matlab script.

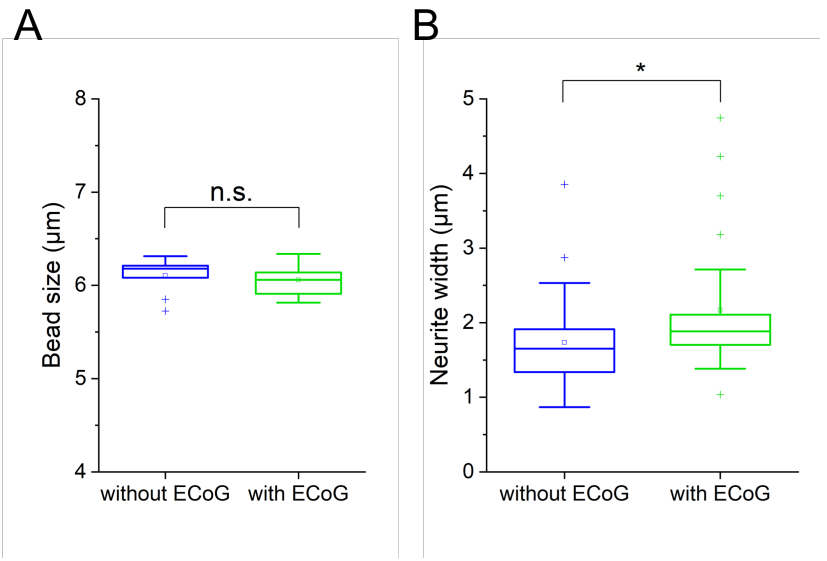

Figure 3: (A) Boxplots of microbead size of the 6.0 µm nominal diameter microbeads. Average size without Parylene HT: 6.11 µm (SD=0.18 µm), with Parylene HT: 6.06 µm (SD=0.16 µm). Mann-Whitney U-test, $p>0.05$, U=39, n=10. (B) Boxplot about the measured in vitro neurite width in a distance between 30 and 70 µm from the cell soma. Average neurite width without Parylene HT: 1.73 µm (SD=0.61 µm, n=29), with Parylene HT: 2.17 µm (SD=0.89 µm, n=26). Mann-Whitney U-test, $p<0.05$, U=234. The bottom and top edges of the boxes indicate the 25th and 75th percentiles. The whiskers extend to the most extreme data points not considered outliers, and the outliers are plotted individually using the '+' symbol (Origin built-in boxplot function).

Thesis 2.2. *I investigated the sensitivity of the proposed recording sites to two-photon illumination. In resonant mode, the used laser power was between 7.7 mW and 132.4 mW, and Z-level was between 0 µm and -30 µm. Based on my analyses on the photoartefact from the different laser power, power values below 12 mW in resonant mode at the device plane (Z = 0) can be safely used without substantial photoelectric artefacts. Laser exposure 10 µm below the device plane does not induce apparent noise in the signal, while low power exposure close to the device plane contributes to parasite peaks in the power density spectra, where the fundamental frequency is corresponding to the frame rate of image acquisition. Focusing the laser beam at Z = -5 µm in resonant and Z = -10 µm in galvanic scanning mode under the ITO recording site apparently suppressed the power density of noise using 33 mW and 13 mW laser power in resonant and galvanic scanning mode, respectively.*

Photoelectric artefacts were evaluated with two-photon microscopy using several scanning modes (galvanic and resonant), depth of focal plane with respect to the device plane (distance) and at various intensity of irradiation (laser power) in Ringer solution. The characteristic patterns of photoelectric artefacts are shown in Figure 4 A. Parylene C samples holding Ti/Au metallization were tested in galvanic scanning as control material to compare the light-induced intensity of artefact signals (Figure 4 B). The power density of artefact

signals in the focal plane (z=0) of indium-tin-oxide surfaces are well below the value in the case of the control metallization. This trend remained stable at various laser powers (Figure 4 B). Power density spectrum also revealed that ITO is more sensitive to galvanic scanning mode than to resonant scanning mode, with respect to light-induced artefacts (Figure 4 C. Regarding the investigations at various depth, it appeared that focusing the laser beam at Z = -5 μm in resonant and at Z = -10 μm in galvanic scanning mode under the ITO recording site apparently suppressed the power density of noise using 33 mW and 13 mW laser power in resonant and galvanic scanning mode, respectively (Figure 4 D).

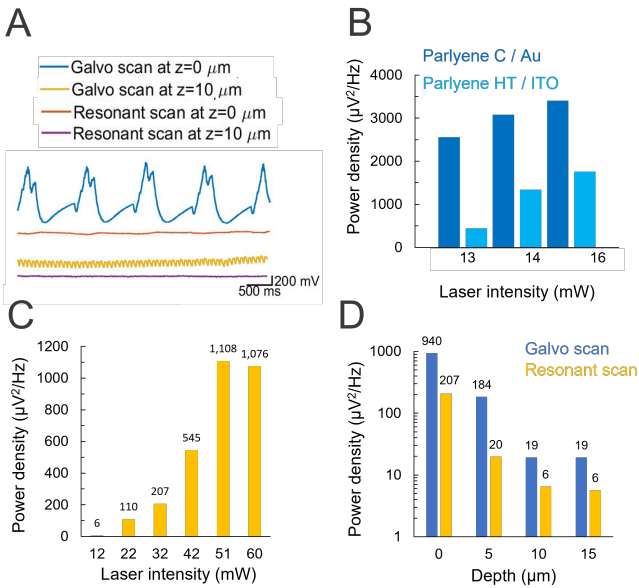

Figure 4: (A) Representative curves on the sensitivity of signal recording to photoelectric artefacts at galvanic and resonant scanning modes measured on the device plane (Z = 0 µm) and at Z = -10 µm. (B) Comparison of the photo artefacts of Parylene C/Ti/Au electrodes and Parylene HT/ITO electrodes at various light intensities at the fundamental harmonic for galvanic scanning (2.11 Hz). (C) Maximum power density of noise using various light intensities on a recording site (Z = 0 µm) at the fundamental harmonic of resonant mode (30.98 Hz). (D) Maximum power density of noise at different distances from the device plane. The laser was focused on the site (Z = 0 µm) and under the site in the shown depth. Laser intensities are 13 mW and 33 mW for galvanic and resonant mode, respectively.

3 Potential applications and benefits

My work has improved the advancement in the technology of in vitro cell culturing microdevices. The results of my work have substantially contributed to the success of the related research project funded by the National Development and Innovation Office (NKFIH) through grant number OTKA NN 116550 (led by Dr Anita Pongrácz). The investigation on transparent microimplants paved the way for the development of new multimodal imaging approaches that recently facilitated network scale monitoring of neural activity in combination with two-photon imaging in awake animals. The results of this thesis constituted an essential part of the research project funded by NKFIH under grant number NKFIH K 120143 and 2017_1.2.1-NKP-2017-00002 (led by Dr Zoltán Fekete). Based on the above work and efforts, a long-term collaboration between Qualia Medical Inc. (Dallas, Texas, USA) has been launched, and using my established characterization tools, evaluation of shape memory polymer based microECoGs are being efficiently carried out.

Acknowledgment

Working in a supportive and inspiring environment is a great privilege. I am grateful for creating such a workplace to my supervisor *Dr. Zoltán Fekete* and motivating me with his enthusiasm. During my work in the Research Group for Implantable Microsystems, he not only helped me finding new solutions and publish them, but gave me great advices how to navigate my career. I would like to thank to *Dr. Anita Pongrácz*, my previous supervisor, to welcoming me to this wonderful team. I am also thankful to my team members, *Dr. Anita Zátonyi, Bence Csernyus, Dr. Ágoston Horváth, Zsófia Lantos, Ebrahim Ismaiel* for the friendly atmosphere and joint research work.

I find the work with collaborators a great advantage. I would like to thank all the help and work for *Dr. Hanna Liliom, Dr. Katalin Schlett* during the investigation of the interaction between astrocytes and micropatterned surfaces. Thanks to *Miklós Madarász* and *Tibor Lőrincz* for the in vitro, in vivo and two-photon experiments. Thanks for the supportive work of the cleanroom staff at the Microsystems Lab in the Centre for Energy Research.

I am thankful to the Doctoral School, especially to *Prof. Gábor Szederkényi*, *Prof. Péter Szolgay* and *Prof. Pongor Sándor* for the opportunity to participate in the doctoral program. I am specially thankful to *Dr. Tivadarné Vida* for her kind help during my doctoral studies.

I would like to thank to my family and friends for their limit-

less support. Special thanks to *János Szőts* for the help in editing my manuscript and all his patience, support and time during these four years.

Finally, I like to thank for the following grants to support my work. The European Union through the grant EFOP-3.6.3-VEKOP-16-2017-00002 co-financed by the European Social Fund is also acknowledged; the KAP19-32003-3.3-ITK grants; the National Brain Research Program (grant: 2017_1.2.1-NKP-2017-00002) and the National Research, Development and Innovation Office (grants: NKFIH K 120143). Also, for the New National Excellence Program of the Ministry for Innovation and Technology (grants: ÚNKP-20-3, ÚNKP-21-3)

Publications of the author

Journal publications

[J1] **Szabó, Á.**, Liliom, H., Fekete, Z., Schlett, K., & Pongrácz, A, "SU-8 microstructures alter the attachment and growth of glial cells in vitro," *Materials Today Communications, 27, 102336*, 2021. Available: `https://doi.org/10.1016/j.mtcomm.2021.102336`.

[J2] Zátonyi, A.*, Madarász, M.*, **Szabó, Á.***, Lőrincz, T., Hodován, R., Rózsa, B., & Fekete, Z., "Transparent, low-autofluorescence microECoG device for simultaneous Ca2+ imaging and cortical electrophysiology in vivo," *Journal of Neural Engineering, 17(1), 016062*, 2020. Available: `https://doi.org/10.1088/1741-2552/ab603f`. *These authors contributed equally.

Conference publication

[C1] Pongrácz A, Barna S, Lukács I, Illés L, Liliom H, Lajer P, Csernyus B, **Szabó Á**, Bérces Z, Fekete Z, Lőw P, Schlett K, "Modification of Glial Attachment by Surface Nanostructuring of SU-8 Thin Films," *Proceedings*. 2(13):1016, 2018. Available: `https://doi.org/10.3390/proceedings2131016`

Other publications

[OP1] Liliom, H., Lajer, P., Bérces, Z., Csernyus, B., **Szabó, Á.**, Pinke, D., Lőw, P., Fekete, Z., Pongrácz, A, & Schlett, K, "Comparing the effects of uncoated nanostructured surfaces on primary neurons and astrocytes," *Journal of Biomedical Materials Research Part A, 107(10), 2350-2359*, 2019. Available: `https://doi.org/10.1002/jbm.a.36743`

[OP2] Csernyus, B., **Szabó, Á.**, Zátonyi, A., Hodován, R., Lázár, C., Fekete, Z., Erőss. L. & Pongrácz, A, "Recent antiepileptic and neuroprotective applications of brain cooling", *Seizure, 82, 80-90*, 2020. Available: `https://doi.org/10.1016/j.seizure.2020.09.018`

[OP3] Csernyus, B., **Szabó, Á.**, Fiáth, R., Zátonyi, A., Lázár, C., Pongrácz, A., & Fekete, Z, "A multimodal, implantable sensor array and measurement system to investigate the suppression of focal epileptic seizure using hypothermia", *Journal of Neural Engineering, 18(4), 0460c3*, 2021. Available: `https://doi.org/10.1088/1741-2552/ac15e6`

[OP4] Fedor, F. Z., Madarász, M., Zátonyi, A., **Szabó, Á.**, Lőrincz, T., Danda, V., Spurgin, L., Manz, C., Rózsa, B., & Fekete, Z, "Soft, Thiolene/Acrylate-Based Electrode Array for Long-Term Recording of Intracranial EEG Signals with Improved Biocompatibility in Mice", *Advanced Materials Technologies, 7, 2100942*, 2021. Available: `https://doi.org/10.1002/admt.202100942`

[OP5] **Szabó, Á.**, Madarász, M., Lantos, Zs., Zátonyi, A., Danda, V.,

Spurgin, L., Manz, C., Rózsa, B., & Fekete, Z, "Transparent thiolene/acrylate based microECoG devices used for concurrent recording of fluorescent Calcium signals and electrophysiology in awake animals", *Advanced Materials Interfaces* in press, 2022.

References

[1] R. Bashir, "Biomems: state-of-the-art in detection, opportunities and prospects," *Advanced Drug Delivery Reviews*, vol. 56, pp. 1565–1586, 9 2004.

[2] V. S. Polikov, P. A. Tresco, and W. M. Reichert, "Response of brain tissue to chronically implanted neural electrodes," *Journal of Neuroscience Methods*, vol. 148, pp. 1–18, 10 2005.

[3] J. K. Nguyen, D. J. Park, J. L. Skousen, A. E. Hess-Dunning, D. J. Tyler, S. J. Rowan, C. Weder, and J. R. Capadona, "Mechanically-compliant intracortical implants reduce the neuroinflammatory response," *Journal of Neural Engineering*, vol. 11, p. 056014, 8 2014.

[4] Z. Fekete and A. Pongrácz, "Multifunctional soft implants to monitor and control neural activity in the central and peripheral nervous system: A review," *Sensors and Actuators B: Chemical*, vol. 243, pp. 1214–1223, 5 2017.

[5] L. J. Tang, M. H. Wang, H. C. Tian, X. Y. Kang, W. Hong, and J. Q. Liu, "Progress in research of flexible mems microelectrodes for neural interface," *Micromachines 2017, Vol. 8, Page 281*, vol. 8, p. 281, 9 2017.

[6] R. Green and M. R. Abidian, "Conducting polymers for neural prosthetic and neural interface applications," *Advanced Materials*, vol. 27, pp. 7620–7637, 12 2015.

[7] S. N. Obaid, R. T. Yin, J. Tian, Z. Chen, S. W. Chen, K. B. Lee, N. Boyajian, A. N. Miniovich, I. R. Efimov, L. Lu, S. N. Obaid, R. T. Yin, J. Tian, Z. Chen, S. W. Chen, K. B. Lee, N. Boyajian, A. N. Miniovich, I. R. Efimov, and L. Lu, "Multifunctional flexible biointerfaces for simultaneous colocalized optophysiology and electrophysiology," *Advanced Functional Materials*, vol. 30, p. 1910027, 6 2020.

[8] W. Yang, Y. Gong, C. Y. Yao, M. Shrestha, Y. Jia, Z. Qiu, Q. H. Fan, A. Weber, and W. Li, "A fully transparent, flexible pedot:pss–ito–ag–ito based microelectrode array for ecog recording," *Lab on a Chip*, vol. 21, pp. 1096–1108, 3 2021.

[9] C. J. Bettinger, R. Langer, and J. T. Borenstein, "Engineering substrate topography at the micro- and nanoscale to control cell function," *Angewandte Chemie International Edition*, vol. 48, pp. 5406–5415, 7 2009.

[10] J. Luo, M. Walker, Y. Xiao, H. Donnelly, M. J. Dalby, and M. Salmeron-Sanchez, "The influence of nanotopography on cell behaviour through interactions with the extracellular matrix – a review," *Bioactive Materials*, vol. 15, pp. 145–159, 9 2022.

[11] D.-H. Kim, P. P. Provenzano, C. L. Smith, and A. Levchenko, "Matrix nanotopography as a regulator of cell function," *Journal of Cell Biology*, vol. 197, no. 3, pp. 351–360, 2012.

[12] E. M. C. Hillman, "Optical brain imaging in vivo: techniques and applications from animal to man," *Journal of biomedical optics*, vol. 12, p. 051402, 9 2007.

[13] C. Im and J. M. Seo, "A review of electrodes for the electrical brain signal recording," *Biomedical Engineering Letters 2016 6:3*, vol. 6, pp. 104–112, 9 2017.

[14] B. A. Wilt, L. D. Burns, E. T. Ho, K. K. Ghosh, E. A. Mukamel, and M. J. Schnitzer, "Advances in light microscopy for neuroscience," *Annual review of neuroscience*, vol. 32, p. 435, 6 2009.

[15] F. Helmchen and W. Denk, "Deep tissue two-photon microscopy," *Nature Methods 2005 2:12*, vol. 2, pp. 932–940, 11 2005.

[16] T. Vignaud, L. Blanchoin, and M. Théry, "Directed cytoskeleton self-organization," *Trends in Cell Biology*, vol. 22, pp. 671–682, 12 2012.

[17] E. K. Yim, E. M. Darling, K. Kulangara, F. Guilak, and K. W. Leong, "Nanotopography-induced changes in focal adhesions, cytoskeletal organization, and mechanical properties of human mesenchymal stem cells," *Biomaterials*, vol. 31, pp. 1299–1306, 2 2010.

[18] H. Y. Lou, W. Zhao, X. Li, L. Duan, A. Powers, M. Akamatsu, F. Santoro, A. F. McGuire, Y. Cui, D. G. Drubin, and B. Cui, "Membrane curvature underlies actin reorganization in response to nanoscale surface topography," *Proceedings of the National Academy of Sciences of the United States of America*, vol. 116, pp. 23143–23151, 11 2019.

[19] M. J. Dalby, M. O. Riehle, S. J. Yarwood, C. D. Wilkinson, and A. S. Curtis, "Nucleus alignment and cell signaling in fibroblasts: Response to a micro-grooved topography," *Experimental Cell Research*, vol. 284, pp. 272–280, 4 2003.

[20] S. Ankam, M. Suryana, L. Y. Chan, A. A. K. Moe, B. K. Teo, J. B. Law, M. P. Sheetz, H. Y. Low, and E. K. Yim, "Substrate topography and size determine the fate of human embryonic stem cells to neuronal or glial lineage," *Acta Biomaterialia*, vol. 9, pp. 4535–4545, 1 2013.

[21] K. Wang, A. Bruce, R. Mezan, A. Kadiyala, L. Wang, J. Dawson, Y. Rojanasakul, and Y. Yang, "Nanotopographical modulation of cell function through nuclear deformation," *ACS Applied Materials and Interfaces*, vol. 8, pp. 5082–5092, 3 2016.